ACS APPLIED MATERIALS & INTERFACES

Research Article

www.acsami.org

Hierarchical Microporous/Mesoporous Carbon Nanosheets for High-Performance Supercapacitors

Antonio B. Fuertes and Marta Sevilla*

Instituto Nacional del Carbón (CSIC), P.O. Box 73, Oviedo 33080, Spain

Ⓢ *Supporting Information*

ABSTRACT: A straightforward one-pot approach for the synthesis of highly porous carbon nanosheets with an excellent performance as supercapacitor electrodes is presented. The procedure is based on the carbonization of an organic salt (i.e., sodium gluconate) at a temperature in the range of 700−900 °C. The carbon nanosheets have a large aspect ratio (length/thickness ≈ 10^2−10^3), a thickness within the range of 40−200 nm, high BET surface areas (S_{BET}) of up to 1390 m^2 g^{-1}, and a porosity with a hierarchical organization in the micropore−mesopore range. Importantly, via an additional activation step, the textural properties can be substantially enhanced (S_{BET} up to 1890 m^2 g^{-1}). Both the nanosheet morphology (short diffusional paths) and the hierarchical microporous/mesoporous pore structure allow the rapid transport of ions throughout the carbonaceous matrix, leading to excellent electrochemical performance. Thus, the hierarchical nanosheets exhibit specific capacitances of up to 140 F g^{-1} at an ultrahigh discharge current of 150 A g^{-1} in 1 M H_2SO_4 and 100 F g^{-1} at 120 A g^{-1} in 1 M $TEABF_4$/AN. The maximum specific power recorded in an aqueous electrolyte is ∼20−30 kW kg^{-1} and ∼90−110 kW kg^{-1} in an organic electrolyte. These promising power characteristics are accompanied by excellent cycling stability.

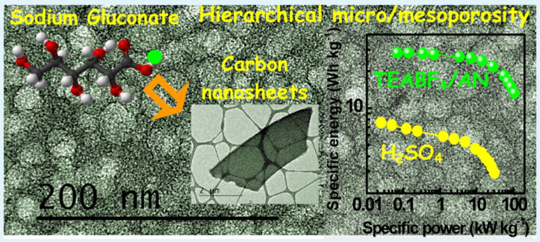

KEYWORDS: *carbon, porosity, supercapacitors, electrode materials, power*

■ INTRODUCTION

Carbon materials are attracting increasing interest in many technological areas, especially those related to energy storage and conversion.[1] For these advanced applications, it is essential that the carbon materials possess an appropriate pore structure and particle architecture. This is especially important in the case of porous carbons that are used as electrodes in electrochemical double-layer capacitors (EDLCs). In these systems, the storage of energy occurs via the accumulation of electrical charges across the electrode/electrolyte interface and, as a consequence, carbons with high surface areas are greatly preferred.[2,3] It has recently been found that the specific capacitance undergoes a sharp increase in carbons with pore sizes of <1 nm.[4,5] This finding shows that, to achieve a high capacitance (high energy density), porous carbons must possess not only a high surface area but also a large number of narrow micropores. Clearly, this type of porosity will severely limit the transport of ions in large particles (>5 μm), and undermine the EDLC performance at high current densities (high power density).[6] To overcome this problem, it is important to design porous carbons with an appropriate architecture combining several properties: (i) a large surface area, (ii) a significant fraction of the pore volume consisting of narrow micropores, (iii) a large number of wide mesopores, and (iv) an effective particle size of <200 nm. In this way, while/whereas properties (i) and (ii) will ensure a high energy density, properties (iii) and (iv) will guarantee short ion-transport times (high power density). Or: In this way, properties (i) and (ii) will ensure a high energy density, while/whereas properties (iii) and (iv) will guarantee short ion-transport times (high power density).

An interesting approach to improve the ion-transport kinetics in microporous carbons has been proposed by Wang et al., who described the fabrication of carbon powders with a hierarchical pore structure that combines macropores, mesopores, and micropores.[7] This pore organization reduces the effective diffusional paths, thereby improving the EDLC performance. Another alternative is to fabricate nanometer-sized porous carbon particles (<200 nm, diffusional path <100 nm). In particular, 2D porous carbon nanosheets with a thickness of <200 nm are an attractive option, because they are easy to synthesize.[8−11] Graphene is a good example of a 2D carbon nanostructure.[12] However, it has been observed that graphene nanosheets have a tendency to aggregate (self-restacking) during the preparation of the electrode, which results in a substantial loss of active surface area and a reduction in electrochemical performance.[13] To solve this problem, the intercalation of several types of carbon nanoparticles between the graphene sheets or the synthesis of graphene sheets with curved morphologies has been investigated.[14−20] However, these procedures require additional steps, which introduces a certain amount of complexity into the synthesis process. In a recent report, Fan et al. described the fabrication of mesoporous carbon nanosheets with a unique pillared architecture and analyzed the

Received: December 15, 2014
Accepted: February 3, 2015
Published: February 12, 2015

DOI: 10.1021/am508794f

EDLC performance of such materials.[21] However, the synthesis procedure is somewhat complex and the carbon particles have a relatively low surface area (<900 m^2 g^{-1}) and a porosity composed exclusively of mesopores (~7 nm). Wang et al. showed that carbon nanosheets obtained by the hydrothermal carbonization of natural fibers, followed by chemical activation with KOH, as electrochemical capacitor electrodes or EC electrodes.[22] Recently, we reported an easy, one-step procedure for the synthesis of highly porous interconnected carbon nanosheets with an excellent performance as supercapacitor electrodes based on the carbonization of an organic salt (i.e., potassium citrate) at a temperature in the range of 750−900 °C.[23] Despite these advances, there is still a need for the development of simple, cost-effective, and "green" approaches to the production of porous carbon nanosheets for high-performance EDLC systems.

In this paper, we present a template-free one-step synthesis method for the fabrication of hierarchical porous carbon nanosheets. These carbon particles satisfy two important conditions necessary that are necessary for their use in EDLC systems: (i) a two-dimensional (2D) morphology with a carbon sheet thickness of <200 nm and (ii) a hierarchical porous structure made up of large mesopores (>10 nm) fully interconnected by narrow micropores (<1 nm). The small thickness of the carbon sheets guarantees short ion-transport times, while the hierarchical pore structure has a double function: the large mesopores act as ion-buffering reservoirs and the micropores accommodate the ion charges that build up the electric double-layer. The procedure for fabricating the hierarchical porous carbon nanosheets is simple, involving the carbonization of sodium gluconate by means of a synthesis strategy recently developed in our laboratory.[24] It should be emphasized that these carbon materials can be easily produced in only one step by using as precursor a widely available inexpensive substance as a precursor.

■ EXPERIMENTAL SECTION

Synthesis of Materials. In a typical synthesis procedure, 3 g of sodium gluconate (Aldrich) was heat-treated in a stainless steel reactor under a nitrogen atmosphere up to the required temperature within the range of 700−900 °C at a heating rate of 3 °C min^{-1} and held at this temperature for 1 h. The resulting black solid residue was then washed with HCl (10%) for the removal of sodium compounds. Finally, the solid was collected by filtration, washed with abundant distilled water, and dried at 120 °C for several hours. The carbon samples were denoted as GNa-*X*, where *X* is the reaction temperature (in °C). The yield of the GNa-*X* samples varied from 22% for GNa-700 to 8.5% for GNa-900.

To increase the porosity of the GNa-based carbons, activated samples were prepared by one of two different procedures: (a) physical activation by carbon gasification with CO_2 or (b) chemical activation with KOH. For physical activation, a GNa-900 sample was gasified with CO_2 at 700 °C for 24 h to reach a burnoff of 35% (gasification rate of <2% h^{-1}). This sample has been denoted as GNa-PA. In the case of chemical activation, a certain amount of GNa-750 carbon was ground thoroughly with KOH (KOH/GNa-750 weight ratio = 3) and heat-treated at 800 °C for 1 h under nitrogen. Finally, the solid residue was washed with HCl (10%) and distilled water. This activated sample has been designated as GNa-CA.

Physical Characterization. Scanning electron microscopy (SEM) images were obtained on a Quanta FEG650 (FEI) instrument, and transmission electron microscopy (TEM) images were recorded on a JEOL (Model JEM 2100-F) apparatus operating at 200 kV. The nitrogen sorption isotherms of the carbon samples were measured at −196 °C using a Micromeritics Model ASAP 2020 sorptometer. The apparent surface area was calculated using the BET method. The total pore volume was determined from the amount of nitrogen adsorbed at a relative pressure (p/p_0) of 0.95, and the micropore volume was determined using an α_s-plot. The mesopore size distributions were determined by means of the Kruk−Jaroniec−Sayari (KJS) method,[25] whereas the micropore size distributions were obtained by using the Quench Solid State Density Functional Theory (QSDFT).[26,27] X-ray diffraction (XRD) patterns were obtained on a Siemens D5000 instrument operating at 40 kV and 20 mA, using CuKα radiation. The Raman spectra were recorded on a Horiba (LabRam HR-800) spectrometer. The source of radiation was a laser operating at a wavelength of 514 nm and at a power of 25 mW. Thermogravimetric analysis (TGA) curves were recorded on a TA Instruments Model Q600 TGA system.

The dc electrical conductivity and the packing density of the carbon powders were determined in a homemade apparatus (four-probe method) by pressing the powders between two plungers into a hollow nylon cylinder (inner diameter of 8 mm), and applying a pressure of 7.1 MPa.

Electrochemical Characterization. Electrodes were prepared by mixing 85 wt % active material with 10 wt % polytetrafluoroethylene (PTFE) binder (Aldrich, 60 wt % suspension in water) and 5% Super P (Timcal). The electrochemical measurements were performed in two-electrode Swagelok-type cells using stainless steel current collectors. Electrochemical capacitors were constructed using two carbon electrodes of comparable mass and thickness (carbon loading in each electrode: ~5 mg cm^{-2}), electrically isolated by a glassy fibrous separator. A 1 M tetraethylammonium tetrafluoroborate salt ($TEABF_4$, electrochemical grade, Sigma−Aldrich) solution in acetonitrile (AN, 99.8%, anhydrous, Sigma−Aldrich) and a 1 M H_2SO_4 aqueous solution were used as electrolytes. The electrochemical characterization was carried out on a computer-controlled potentiostat (Biologic VMP3 multichannel generator).

Electrochemical impedance spectroscopy (EIS) was performed at open circuit voltage (i.e., 0 V) within the frequency range of 1 mHz to 100 kHz and a 10 mV AC amplitude. Nyquist plots and plots of the dependence of capacitance on frequency were recorded to characterize the impedance of the tested samples. The specific gravimetric capacitance of a single electrode, C_{EIS} (F/g), was calculated according to the following formula and normalized with respect to the specific gravimetric capacitance at 1 mHz:

$$C_{\mathrm{EIS}} = \frac{2|\mathrm{Im}(Z)|}{2\pi f[(\mathrm{Im}(Z))^2 + (\mathrm{Re}(Z))^2]m}$$

where f is the operating frequency (Hz), and Im(Z) and Re(Z) are the imaginary and real components of the total device resistance (expressed in ohms). The relaxation time constant (τ_0), which separates the capacitive behavior and the resistive behavior of the supercapacitor, was deduced from the frequency f_0 as follows: $\tau_0 = 1/f_0$, where f_0 is the frequency at which 50% of the capacitance can be accessed.

Cyclic voltammetry was conducted in the 0−2.7 V range for the organic electrolyte and 0−1 V range for the aqueous electrolyte at increasing sweep rates from 1 to 3000 mV s^{-1}. The specific gravimetric capacitance of one electrode was calculated from the plateau (far from the transient regions) in the graph of specific capacitance versus voltage.

Galvanostatic charge/discharge cycling was performed in the same voltage ranges as cyclic voltammetry at current densities in the 0.05−150 A g^{-1} range, on the basis of the active mass of the working electrode. The specific gravimetric capacitance on a single-electrode basis was determined from the slope of the discharge voltage profile (dV/dt) using the formula

$$C_{\mathrm{sp}} = \frac{2I}{(\mathrm{d}V/\mathrm{d}t)m}$$

where I is the current and m is the mass of carbon material in one electrode.

To trace the Ragone plots, the specific energy (Wh kg^{-1}) was calculated using the following formula:

$$E = \frac{1}{2} C_{\mathrm{cell}} \Delta V_{\mathrm{d}}^{2}$$

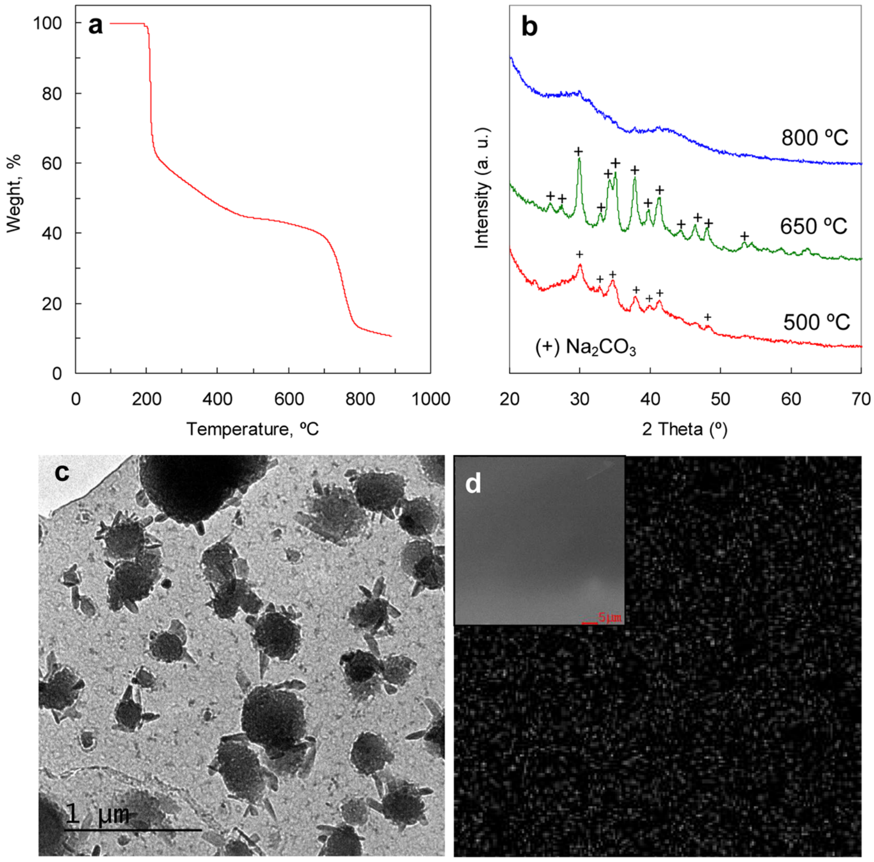

Figure 1. (a) TGA profile of sodium gluconate (N_2 atmosphere, heating rate of 3 °C/min), (b) XRD patterns for the sodium gluconate samples heat-treated at several temperatures, (c) TEM image of the sample carbonized at 650 °C, and (d) EDX mapping of sodium in a carbon nanosheet (shown as an inset).

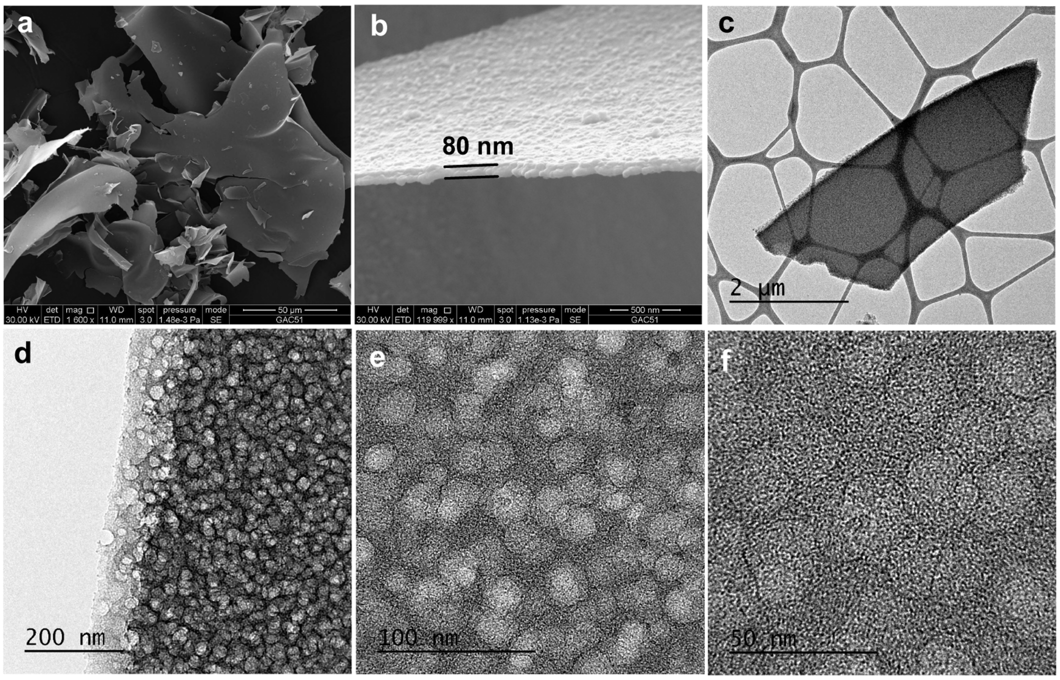

Figure 2. (a, b) SEM and (c, d, e, f) TEM images of the carbon nanosheets obtained by the heat treatment of sodium gluconate at 850 °C.

where C_{cell} is the specific capacitance of the total cell (F g^{-1}) and ΔV_d is the operation voltage ($\Delta V_d = V_{max}$ − IR drop).

The specific power (kW kg^{-1}) was calculated by means of the formula:

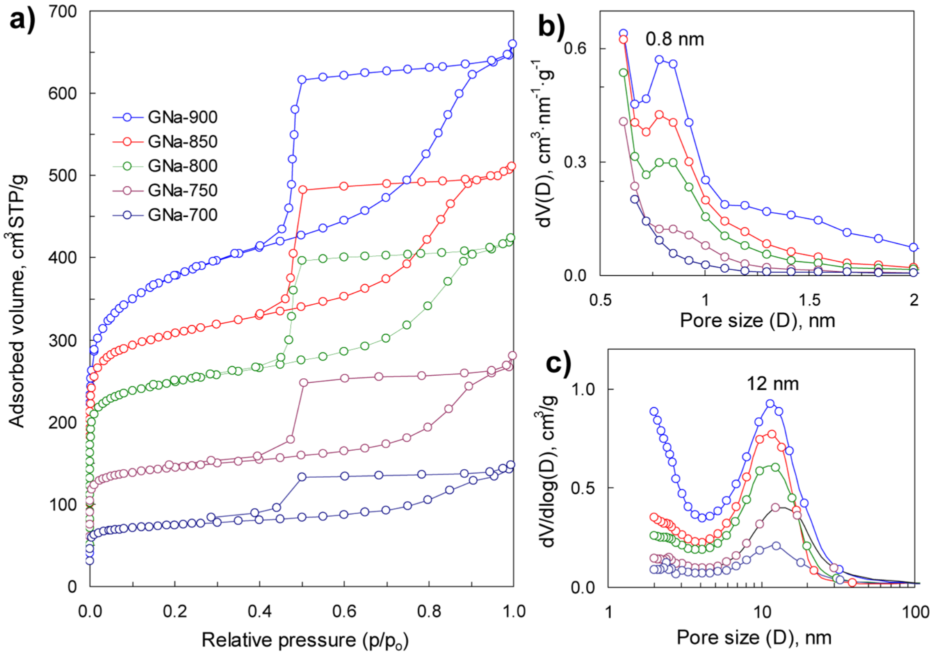

Figure 3. (a) Nitrogen sorption isotherms, (b) micropore size distributions (QSDFT method), and (c) mesopore size distributions (Kruk–Jaroniec–Sayari (KJS) method) corresponding to the carbon nanosheets prepared at different carbonization temperatures.

$$P = \frac{E}{\Delta t_d}$$

where Δt_d is the discharge time.

The self-discharge and leakage current were evaluated by constant load tests, which consisted of charging at a rate of 10 A g^{-1} up to the required voltage, i.e., 0.8/1 V in H_2SO_4 and 2.0/2.7 V in $TEABF_4$/AN. The voltage was then kept stable for 2 h. This was followed by a period of several hours at open circuit when the dependence of cell voltage on time was recorded.

RESULTS AND DISCUSSION

Formation and Structural Characteristics of the Microporous/Mesoporous Carbon Nanosheets. The heat-treatment of sodium gluconate under an inert atmosphere leads directly to 2D porous carbon nanosheets that contain a certain amount of inorganic impurities (i.e., sodium compounds), which can be easily removed by washing with diluted HCl. These nanosheets have a well-developed porosity (*vide infra*), which is generated because of the reactions that occur between the carbonaceous material and the inorganic compounds during the carbonization step. The decomposition of sodium gluconate was monitored by means of thermogravimetric analysis (TGA). The TGA curve in Figure 1a clearly shows two weight loss steps in the temperature ranges of 200–480 °C and 700–800 °C. The first weight loss step is associated with the decomposition of the organic moiety, which occurs simultaneously to the formation of sodium carbonate. X-ray diffraction (XRD) patterns reveal the presence of this compound in the samples obtained at 500 and 650 °C (Figure 1b). Moreover, a TEM image of a sample at 650 °C shows Na_2CO_3 crystallites deposited on the surface of a carbonaceous sheet (Figure 1c). The second weight loss step (700–800 °C) is the consequence of several simultaneous reactions. First, the decomposition of the sodium carbonate ($Na_2CO_3 \rightarrow CO_2 + Na_2O$) takes place, as can be deduced from the XRD pattern corresponding to a sample prepared at 800 °C (Figure 1b). The CO_2 released then reacts with carbon ($CO_2 + C \rightarrow 2CO$), while the Na_2O is reduced ($Na_2O + C \rightarrow 2Na + CO$). Both processes lead to the formation of a large number of micropores.[28−30] Furthermore, the metallic sodium produced generates additional porosity, because it is intercalated between the graphene layers, causing the swelling and disruption of the carbon microstructure.[31,32] This is supported by the EDX-mapping analysis, which reveals that sodium is uniformly distributed throughout the carbon nanosheets, suggesting that it is intercalated within the carbon framework (Figure 1d).

Figure 2 displays SEM and TEM images of the carbon particles obtained by the carbonization of sodium gluconate. It can be seen that they consist of crumpled sheets of a very large aspect ratio, with a length of up to more than 100 μm (see Figures 2a) and a thickness within the 40–200 nm range (see Figure 2b and Figure S1 in the Supporting Information). The sheets are highly porous as can be inferred from the TEM photomicrographs in Figures 2c–f and Figure S2 in the Supporting Information. These images reveal that the carbon nanosheets have two pore systems with a hierarchical organization, consisting of spherical nanovoids of ~10–20 nm (mesopores) (see Figures 2d and 2e) interconnected by narrow micropores, as illustrated by the photomicrographs displayed in Figure 2f and in Figure S2d in the Supporting Information. This pore organization clearly indicates that the mesopores have a cagelike structure (i.e., large voids with narrow entrances).

The carbon nanosheets have a disordered structure, as can be deduced from the fast Fourier transform (FFT) pattern in Figure S2 in the Supporting Information, and also from the XRD pattern and Raman spectrum in Figure S3 in the Supporting Information, which are typical of carbonaceous materials with an amorphous structure. Chemical analysis of the carbon nanosheets revealed that they have a large oxygen content of ~19 wt %, which is independent of the carbonization temperature (see Table S1 in the Supporting Information).

Nitrogen physisorption measurements were performed to analyze the textural characteristics of the carbon nanosheets obtained by the carbonization of sodium gluconate at several temperatures in the range of 700–900 °C. The N_2 sorption isotherms and the pore size distributions corresponding to the micropores and mesopores are shown in Figures 3a, 3b, and 2b, respectively. The adsorption profiles in Figure 3a show that the isotherms are a combination of Type I (typical of microporous carbons) and Type IV (characteristic of mesoporous materials). Interestingly, the sorption isotherms exhibit a broad hysteresis loop with a sharp closure (Type H2 hysteresis loop), which is typical of materials that possess large mesopores with a cagelike structure (small entrances and large interiors).[33,34] This result is coherent with the pore structure shown in the TEM images, which revealed a porosity made up of two pore systems with a hierarchical organization. The presence of two types of pores is confirmed by means of the pore size distributions deduced by the QSDFT method in the case of the micropores (Figure 3b) and the KJS method in the case of the mesopores (Figure 3c). Independent of the carbonization temperature, the mesopores have a size centered at ~12 nm, while the micropores exhibit a maximum at ~0.8 nm. The textural parameters of the carbons synthesized at several temperatures in the range of 700−900 °C are listed in Table 1. These results show that the carbon nanosheets have high Brunauer−Emmett−Teller (BET) surface areas, whose values increase with the carbonization temperature, from $S_{BET} = 280$ m^2 g^{-1} (700 °C) to $S_{BET} = 1390$ m^2 g^{-1} (900 °C). Similarly, the pore volumes increase from 0.21 cm^3 g^{-1} (700 °C) to 0.99 cm^3 g^{-1} (900 °C). Interestingly, the porosity of these carbons is almost equally distributed between the micropores and mesopores. For example, in the case of the GNa-850 sample, the micropore and mesopore volumes are similar, with values of 0.40 cm^3 g^{-1} and 0.47 cm^3 g^{-1} respectively (see Table 1).

Table 1. Textural Properties of Microporous/Mesoporous Carbon Nanosheets

sample code	S_{BET} (m^2 g^{-1})	V_p (cm^3 g^{-1})[a]	V_{micro} (cm^3 g^{-1})[b]	V_{meso} (cm^3 g^{-1})[c]
GNa-700	280	0.21	0.10	0.11
GNa-750	560	0.40	0.18	0.22
GNa-800	960	0.64	0.30	0.34
GNa-850	1280	0.87	0.40	0.47
GNa-900	1390	0.99	0.44	0.55
GNa-PA	1630	1.14	0.57	0.57
GNa-CA	1890	1.33	0.69	0.64

[a]Pore volume at $p/p_0 \approx 0.95$. [b]Micropore volume determined by the α_s-plot technique. [c]Mesopore volume obtained from the difference between pore volume (V_p) and micropore volume (V_{micro}): $V_{meso} = V_p - V_{micro}$.

The pore volume of the carbon nanosheets was increased by using two well-established activation procedures: physical activation with CO_2 and chemical activation with KOH. The TEM images in Figures 4a and 4b show that the activated samples retain their nanosheet morphology and hierarchical porosity with two interconnected pore systems in the mesopore and micropore ranges. The HRTEM microphotograph in Figure 4c, taken at the edge of a GNa-CA nanosheet, shows a microporous network that is composed of randomly oriented narrow micropores. Furthermore, the N_2 sorption isotherms of the activated materials have the same shape as that of the as-prepared carbon nanosheets (see Figure 4d). However, the BET surface area and the pore volumes of the activated samples have increased significantly to 1530 m^2 g^{-1} and 1.14 cm^3 g^{-1} for the CO_2-activated carbon (GNa-PA), and 1890 m^2 g^{-1} and 1.33 cm^3 g^{-1} in the case of the KOH-activated carbon (GNa-CA), respectively (see Table 1). Moreover, the pore size distributions for the micropores (Figure 4e) and mesopores (Figure 4f) are similar to those of the as-prepared samples, except for the appearance of a large number of micropores and the increase in the size of the mesopores up to 20 nm for GNa-PA and up to 30 nm in the case of GNa-CA. Interestingly, in the case of the activated carbon nanosheets, the micropore and mesopore volumes have increased by a similar extent and, as a consequence, the porosity of these samples (as in the case of the nonactivated materials) is also equally distributed between the micropores and mesopores (see Table 1).

Electrochemical Performance of the Carbon Nanosheets. The new carbon nanosheets presented in this work have a unique structure that combines a very small thickness (diffusional paths of <100 nm) with a large surface area of up to ~1900 m^2 g^{-1} and a hierarchical porosity consisting of large spherical mesopores (~10−30 nm) interconnected by narrow micropores (<1 nm). Furthermore, they possess a relatively good electronic conductivity (i.e., ~1−3 S cm^{-1}) (see Table S2 in the Supporting Information). Because of these properties, they can be expected to exhibit an excellent behavior as electrodes for advanced electrochemical capacitors. To confirm this, the electrochemical performance of these carbon samples was measured in organic (1 M $TEABF_4$/AN) and aqueous (1 M H_2SO_4) electrolytes using a wide range of sweep rates and discharge currents.

The first evidence of fast electron/ion transport within the structure of the materials developed was provided by electrochemical impedance spectroscopy (EIS). It was found that the hierarchical nanosheet-based supercapacitors are characterized by small relaxation time constants of 0.7−1.6 s in H_2SO_4 electrolyte and 1.2−2.3 s in $TEABF_4$/AN electrolyte (see Table S2 in the Supporting Information), as deduced from the variation in normalized capacitance with frequency (see Figures S4a and S4b in the Supporting Information). Significantly, such time constant values in the organic electrolyte are much lower than those of porous carbons with a granular morphology, such as the commercial activated carbon Supra DLC-50 (8.5 s),[23] advanced activated carbons (>10 s),[35] and carbide-derived carbons (>5 s).[4,36,37] On the other hand, the time constant values in the aqueous electrolyte are similar to, or smaller than, those of granular ordered hierarchical micro-mesoporous material carbons (1.4−2.5 s),[38] 3D hierarchical porous carbon (6.7 s),[39] and Supra DLC-50 (1.7 s). These data confirm facile ion transport resulting from short ion diffusion paths in these carbon nanosheets. Further proof of the low resistance to the transport of ions within the porous structure is provided by the value of the equivalent distributed resistance (EDR), which is calculated by performing a linear projection of the vertical portion of the Nyquist plot at low frequencies to the real axis and subtracting the equivalent series resistance (ESR) (see Figure S4c in the Supporting Information).[40] Thus, the EDR value is as low as 0.08 Ω in H_2SO_4 and 0.66 Ω in TEABF4/AN; these are values that are substantially lower than those of ordered hierarchical microporous/mesoporous carbons,[38] mesoporous carbon microspheres (diameter <500 nm),[41] or porous graphitic carbon nanosheets.[8] The low values of ESR and EDR will allow a smaller tradeoff between energy and power and higher specific powers, as will be demonstrated below.

The EIS findings have been confirmed by cyclic voltammetry experiments. Thus, it can be seen in Figure 5 that the cyclic voltammograms for both electrolytes have a rectangular shape, which is typical of double-layer capacitors up to high scan rates of

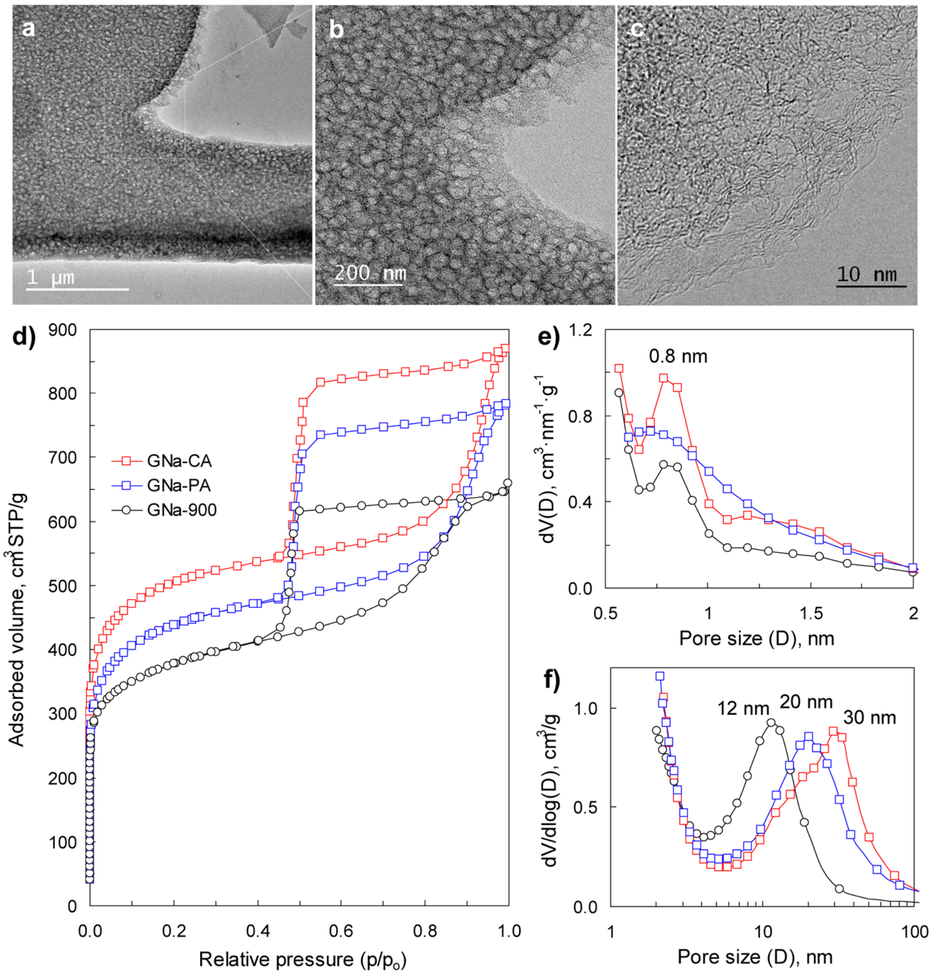

Figure 4. (a, b, c) TEM images of chemically activated carbon nanosheets GNa-CA. (d) Nitrogen sorption isotherms, (e) micropore size distributions (QSDFT method), and (f) mesopore size distributions (KJS method) of the post-activated-carbon nanosheets GNa-CA and GNa-PA.

500−1000 mV s^{-1}. Only at very large sweep rates of 2000−3000 mV s^{-1}, is charge propagation delayed when the voltage sweep is reversed. This leads to a weak sweep rate dependency of capacitance, as shown in Figure S5 in the Supporting Information. It is worth noting that the physically activated GNa-PA sample shows the best rate performance in organic electrolyte, but the worst behavior in aqueous electrolyte. We attribute this behavior to its somewhat hydrophobic character (poor wettability in water), because of its low oxygen content (5.2 wt % O, Table S1 in the Supporting Information). This hinders ion diffusion within the porosity in H_2SO_4. By contrast, these hydrophobic properties are beneficial in an aprotic medium (i.e., $TEABF_4$/AN) and in $TEABF_4$/AN, the GNa-PA carbon shows an excellent electrochemical performance with high specific capacitance values (see Figure S5b in the Supporting Information).

The excellent rate performance of the hierarchical micro-mesoporous materials carbon nanosheets in aqueous/organic electrolytes has been confirmed by galvanostatic charge−discharge experiments. Indeed, the results in Figure 6a show that, for a 1200-fold discharge rate increase in $TEABF_4$/AN, i.e., from 0.1 to 120 A g^{-1} (drain time = 0.34−0.84 s), the capacitance fading of the activated nanosheets is as low as 13%−25% (∼45% for pristine GNa-900 nanosheets). In aqueous electrolyte (1 M H_2SO_4), the behavior of the GNa-CA sample is especially remarkable, with a capacitance fading of only ∼35% at 120 A g^{-1} (drain time = 0.2−0.6 s) (see Figure 6b). As can be seen from the data in Figure 6c, these capacitance losses are lower than those of other advanced carbon materials, such as hierarchical porous graphitic carbon (44% at 50 A g^{-1} in KOH),[7] microporous carbon nanoplates (62% at 70 A g^{-1} in H_2SO_4 and 60% at 40 A g^{-1} in $BMIMBF_4$/AN),[10] 3D microporous conducting carbon beehive (42% at 30 A g^{-1} in H_2SO_4),[42] porous graphene-like nanosheets (31% at 30 A g^{-1} in KOH),[11] N-doped porous graphitic carbon (35−45% at 30 A g^{-1} in KOH),[43] or human hair-derived carbon flakes (65% at 10 A g^{-1} in 1 M $LiPF_6$ EC/DEC).[44] Especially outstanding is the behavior of the GNa-CA carbon that exhibits in 1 M H_2SO_4 a specific capacitance as high as 140 F g^{-1} (54 F cm^{-3}) at a ultrahigh discharge current of 150 A g^{-1} and ∼100 F g^{-1} (∼40 F cm^{-3}) at 120 A g^{-1} in 1 M $TEABF_4$. These results demonstrate the excellent rate capability of the hierarchical micro-mesoporous materials carbon nanosheets synthesized in this study, especially of the activated ones, which combine a large ion storage capacity with an enhanced ion transport capability. It should be noted that, excluding the anomalous behavior of GNa-PA, the capacitance loss of the materials is larger in H_2SO_4 than in $TEABF_4$ for discharge currents lower than 5 A g^{-1}; however, for larger discharge currents, the capacitance loss is similar in both electrolytes. This result suggests pseudo-capacitance phenomena in H_2SO_4, whose kinetics are slower than double-layer formation and therefore play a role only at low discharge currents. This agrees with the

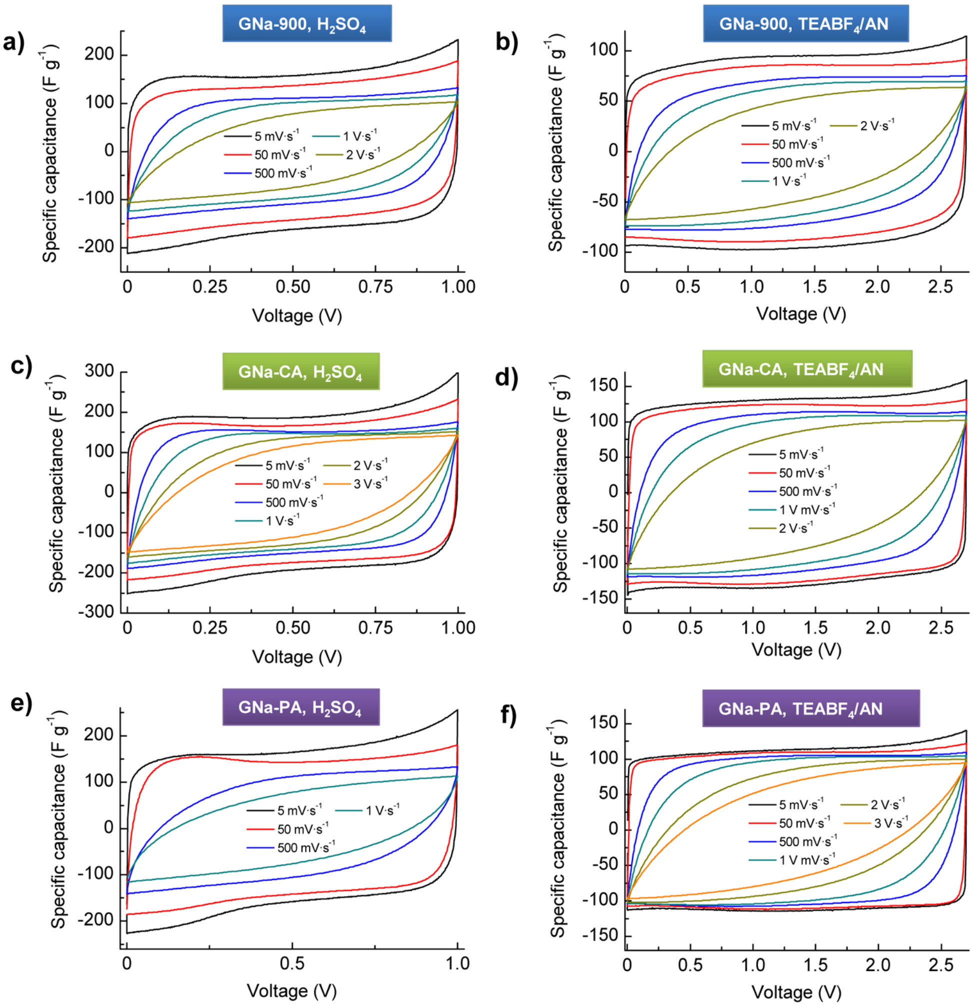

Figure 5. Cyclic voltammograms at increasing sweep rates corresponding to the porous carbon nanosheets in (a, c, e) a 1 M H_2SO_4 solution and (b, d, f) a 1 M $TEABF_4$ solution at ambient temperature.

larger surface-area-normalized capacitances measured at low discharge current (0.1 A g^{-1}) in H_2SO_4 (10.9−12.8 μF cm^{-2}), in comparison to $TEABF_4$ (∼6.9 μF cm^{-2} in 1 M $TEABF_4$).

The high power handling ability of the nanosheets can be clearly visualized in the Ragone plot in Figure 6d. Thus, specific powers well above the Partnership for a New Generation of Vehicles (PNGV) power target[7] are achieved in both types of electrolyte. The highest specific power in an aqueous electrolyte is ∼20−30 kW kg^{-1}/∼9−16 kW L^{-1} (specific energy of ∼1−3 Wh kg^{-1}/∼0.4−1.1 Wh L^{-1}), whereas in an organic electrolyte, a 4-fold increase is registered, i.e., ∼90−110 kW kg^{-1}/∼41−46 kW L^{-1} (specific energy of ∼7−13 Wh kg^{-1}/∼3−6 Wh L^{-1}). On the other hand, in the case of the PNGV power target (i.e., 15 kW kg^{-1}), the amount of energy stored in the supercapacitors is 2−4 Wh kg^{-1} in an aqueous electrolyte and 16−26 Wh kg^{-1} in an organic electrolyte. A comparison of the energy and power characteristics of these materials with those of the best performing carbon materials in the literature is presented in Figure S6 in the Supporting Information. The materials synthesized in this study comfortably surpass the PNGV target, regardless of the electrolyte used, whereas few materials in the literature are able to meet the target and if they do, it is mainly for the organic electrolyte.

The stability of the supercapacitors prepared was examined by charge−discharge cycling at high rates (i.e., 10 A g^{-1}) for 10 000 cycles for a cell voltage of 1 V in an aqueous electrolyte and 2.7 V in an organic electrolyte. A supercapacitor is usually considered, by manufacturers, to be out of service when the initial capacitance has been reduced by 20% or the ESR has increased by 100%.[45] In the case of the microporous/mesoporous carbon nanosheets presented here, the capacitance loss is in the range of 3%−5% (see Figure 7a), whereas the increase in DC ESR is 10% (Figure 7c) after 10 000 cycles in 1 M H_2SO_4. In comparison, in 1 M $TEABF_4$/AN, the capacitance loss is in the range of 9%−13% (Figure 7b) while the increase in DC ESR is also 10% (Figure 7d). Both end-of-life criteria are well below the limits established by the manufacturers, proving the robustness of these carbon nanosheet-based supercapacitors. In addition, we analyzed self-discharge and leakage current phenomena, since these are important when evaluating the performance of a supercapacitor with a back-up function, where it needs to be fully charged for long periods of time. The evaluation of both parameters was performed after long-term cycling through constant load tests for 2 h at the required voltage (1 V in H_2SO_4 and 2.7 V in $TEABF_4$/AN), followed by an open-circuit period. The results are shown in Figures 7e and 7f for GNa-CA in H_2SO_4 and GNa-PA in $TEABF_4$/AN, respectively. The leakage current values in H_2SO_4 are only ∼6−7 mA g^{-1}, whereas self-discharge is 30% after 8 h. In the case of the organic electrolyte, both leakage current and self-discharge values are higher, because they are dependent on the

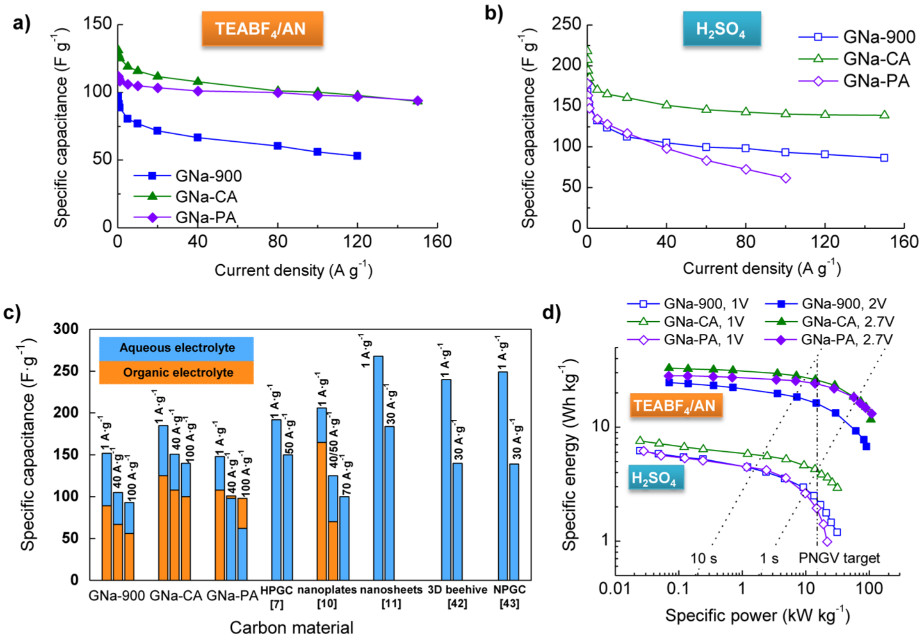

Figure 6. Rate performance evaluated by charge/discharge testing in (a) 1 M TEABF$_4$ solution and (b) 1 M H$_2$SO$_4$ solution at ambient temperature. (c) Comparison of specific capacitances at different discharge rates for a variety of advanced carbon materials. (d) Ragone plot (the vertical dash-dotted line represents the Partnership for a New Generation of Vehicles (PNGV) power target of 15 kW kg^{-1}, in terms of electrode active material weight).

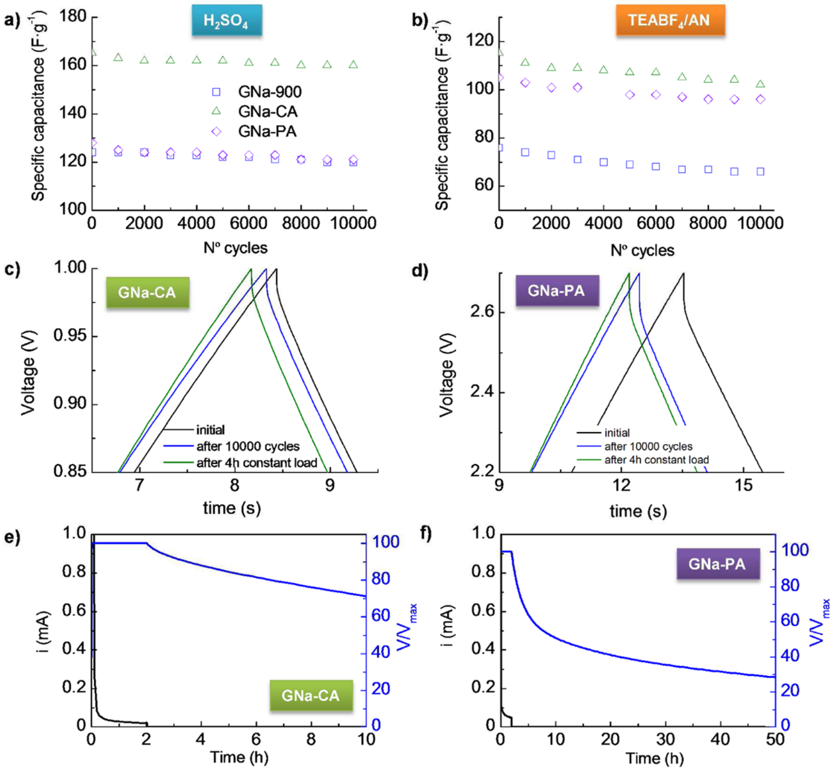

Figure 7. Long-term galvanostatic cycling at 10 A g^{-1}: (a) 1 M H$_2$SO$_4$, cell voltage = 1 V and (b) 1 M TEABF$_4$/AN, cell voltage = 2.7 V. High-magnification of the galvanostatic charge/discharge voltage profiles at 10 A g^{-1}: (c) GNa-CA in 1 M H$_2$SO$_4$ and (d) GNa-PA in 1 M TEABF$_4$/AN. Leakage current and self-discharge: (e) 1 M H$_2$SO$_4$, cell voltage = 1 V, GNa-CA and (f) 1 M TEABF$_4$/AN, cell voltage = 2.7 V, GNa-PA.

voltage applied.[46] They are ∼15−20 mA g^{-1} and 30% after 2−4 h, respectively. If the constant load test is carried out at 2 V, the leakage current decreases to 9−14 mA mg^{-1} and the voltage drop is 30% after 8−10 h (see Figure S7 in the Supporting Information). These data are in the range of values reported for other supercapacitors, such as those based on templated mesoporous carbons,[47] highly porous KOH-activated carbons,[48] or prototype packed cells.[49] Finally, it is worth pointing out that, after the constant load tests (2 h at 0.8 V plus 2 h at 1 V in H$_2$SO$_4$, and 2 h at 2 V plus 2 h at 2.7 V in TEABF$_4$/AN), the capacitance decreased by only ∼1% without any increase in DC ESR in either of the electrolytes, as can be seen in Figures 7c and 7d. This result suggests that these materials may also be robust enough to withstand potentiostatic floating for long periods of time.

CONCLUSIONS

In summary, we have reported a novel and simple approach for producing highly porous carbon nanosheets. These carbon nanosheets are produced by the direct carbonization of sodium gluconate at temperatures in the range of 700−900 °C. In this way, the pyrolysis of the organic moiety and the generation of porosity in the resulting carbon can be integrated in only one step. The resulting carbon nanosheets have a large aspect ratio (length/thickness of $\sim 10^2-10^3$), a thickness in the range of 40−200 nm, and a porosity with a hierarchical organization consisting of large spherical mesopores of ∼12 nm that are interconnected by narrow micropores of <1 nm. In addition, we have demonstrated that the textural properties of these carbonized samples (S_{BET} values up to 1390 $m^2\ g^{-1}$) can be substantially improved by means of an additional activation step (S_{BET} up to 1890 $m^2\ g^{-1}$) without modifying either the morphology of the nanosheets or the hierarchical organization of the porosity. Both the nanosheet morphology (short diffusional paths) and the hierarchical microporous/mesoporous pore structure allow the rapid transport of ions throughout the carbonaceous matrix, resulting in an excellent electrochemical performance. As a result, the hierarchical nanosheets are able to handle ultrahigh discharge current densities of 150 A g^{-1} in both aqueous (H_2SO_4) and organic ($TEABF_4$/AN) electrolytes, exhibiting specific capacitances of up to 140 and 94 F g^{-1}, respectively. In this way, these materials are able to deliver a high specific energy of up to 4 Wh kg^{-1} in aqueous electrolyte and up to 26 Wh kg^{-1} in organic electrolyte at a specific power of 15 kW kg^{-1}. The energy and power characteristics described above are further reinforced by an excellent resistance to both cycling and potentiostatic floating. In short, the novel route presented in this paper is simple and effective for the large-scale production of porous carbon nanosheets destined for use in high-performance supercapacitors.

ASSOCIATED CONTENT

Ⓢ Supporting Information

Tables gathering the chemical composition of the materials, and the electronic conductivity and relaxation time constant of the supercapacitors; SEM and TEM images; FTT spectrum and HRTEM photomicrograph; XRD pattern and Raman spectrum; graph of variation of normalized capacitance with frequency and Nyquist plots in the different electrolytes; graph of rate performance evaluated by cyclic voltammetry in the different electrolytes; Ragone plot showing a comparison of the best performing carbon materials that can be found in the scientific literature; graph of leakage current and self-discharge in 1 M TEABF4/AN at a cell voltage of 2 V. This material is available free of charge via the Internet at http://pubs.acs.org.

AUTHOR INFORMATION

Corresponding Author

*E-mail: martasev@incar.csic.es.

Notes

The authors declare no competing financial interest.

ACKNOWLEDGMENTS

This research work was supported by the Spanish Ministerio de Economía y Competitividad (MAT2012-31651). M.S. thanks the Spanish MINECO for her Ramón y Cajal contract.

REFERENCES

(1) Sevilla, M.; Mokaya, R. Energy Storage Applications of Activated Carbons: Supercapacitors and Hydrogen Storage. *Energy Environ. Sci.* **2014**, *7*, 1250−1280.

(2) Béguin, F.; Presser, V.; Balducci, A.; Frackowiak, E. Carbons and Electrolytes for Advanced Supercapacitors. *Adv. Mater.* **2014**, *26*, 2219−2251.

(3) Yan, J.; Wang, Q.; Wei, T.; Fan, Z. Recent Advances in Design and Fabrication of Electrochemical Supercapacitors with High Energy Densities *Adv. Energy Mater.* **2014**, *4*, DOI: 10.1002/aenm.201300816.

(4) Chmiola, J.; Yushin, G.; Gogotsi, Y.; Portet, C.; Simon, P.; Taberna, P. L. Anomalous Increase in Carbon Capacitance at Pore Sizes Less than 1 Nanometer. *Science* **2006**, *313*, 1760−1763.

(5) Raymundo-Piñero, E.; Kierzek, K.; Machnikowski, J.; Béguin, F. Relationship between the Nanoporous Texture of Activated Carbons and their Capacitance Properties in Different Electrolytes. *Carbon* **2006**, *44*, 2498−2507.

(6) Portet, C.; Yushin, G.; Gogotsi, Y. Effect of Carbon Particle Size on Electrochemical Performance of EDLC. *J. Electrochem. Soc.* **2008**, *155*, A531−A536.

(7) Wang, D.-W.; Li, F.; Liu, M.; Lu, G. Q.; Cheng, H.-M. 3D Aperiodic Hierarchical Porous Graphitic Carbon Material for High-Rate Electrochemical Capacitive Energy Storage. *Angew. Chem., Int. Ed.* **2008**, *47*, 373−376.

(8) Wang, L.; Mu, G.; Tian, C.; Sun, L.; Zhou, W.; Yu, P.; Yin, J.; Fu, H. Porous Graphitic Carbon Nanosheets Derived from Cornstalk Biomass for Advanced Supercapacitors. *ChemSusChem* **2013**, *6*, 880−889.

(9) Jin, Z.-Y.; Lu, A.-H.; Xu, Y.-Y.; Zhang, J.-T.; Li, W.-C. Ionic Liquid-Assisted Synthesis of Microporous Carbon Nanosheets for Use in High Rate and Long Cycle Life Supercapacitors. *Adv. Mater.* **2014**, *26*, 3700−3705.

(10) Yun, Y. S.; Cho, S. Y.; Shim, J.; Kim, B. H.; Chang, S.-J.; Baek, S. J.; Huh, Y. S.; Tak, Y.; Park, Y. W.; Park, S.; Jin, H.-J. Microporous Carbon Nanoplates from Regenerated Silk Proteins for Supercapacitors. *Adv. Mater.* **2013**, *25*, 1993−1998.

(11) Sun, L.; Tian, C.; Li, M.; Meng, X.; Wang, L.; Wang, R.; Yin, J.; Fu, H. From Coconut Shell to Porous Graphene-like Nanosheets for High-Power Supercapacitors. *J. Mater. Chem. A* **2013**, *1*, 6462−6470.

(12) Cao, X.; Yin, Z.; Zhang, H. Three-Dimensional Graphene Materials: Preparation, Structures and Application in Supercapacitors. *Energy Environ. Sci.* **2014**, *7*, 1850−1865.

(13) Stoller, M. D.; Park, S.; Zhu, Y.; An, J.; Ruoff, R. S. Graphene-Based Ultracapacitors. *Nano Lett.* **2008**, *8*, 3498−3502.

(14) Lei, Z.; Christov, N.; Zhao, X. S. Intercalation of Mesoporous Carbon Spheres between Reduced Graphene Oxide Sheets for Preparing High-Rate Supercapacitor Electrodes. *Energy Environ. Sci.* **2011**, *4*, 1866−1873.

(15) Zhang, L. L.; Xiong, Z.; Zhao, X. S. Pillaring Chemically Exfoliated Graphene Oxide with Carbon Nanotubes for Photocatalytic Degradation of Dyes under Visible Light Irradiation. *ACS Nano* **2010**, *4*, 7030−7036.

(16) Wang, G.; Sun, X.; Lu, F.; Sun, H.; Yu, M.; Jiang, W.; Liu, C.; Lian, J. Flexible Pillared Graphene-Paper Electrodes for High-Performance Electrochemical Supercapacitors. *Small* **2012**, *8*, 452−459.

(17) Xu, Z.; Li, Z.; Holt, C. M. B.; Tan, X.; Wang, H.; Amirkhiz, B. S.; Stephenson, T.; Mitlin, D. Electrochemical Supercapacitor Electrodes from Sponge-like Graphene Nanoarchitectures with Ultrahigh Power Density. *J. Phys. Chem. Lett.* **2012**, *3*, 2928−2933.

(18) Liu, C.; Yu, Z.; Neff, D.; Zhamu, A.; Jang, B. Z. Graphene-Based Supercapacitor with an Ultrahigh Energy Density. *Nano Lett.* **2010**, *10*, 4863−4868.

(19) Yang, X.; Zhu, J.; Qiu, L.; Li, D. Bioinspired Effective Prevention of Restacking in Multilayered Graphene Films: Towards the Next

Generation of High-Performance Supercapacitors. *Adv. Mater.* **2011**, *23*, 2833−2838.

(20) Yan, J.; Liu, J.; Fan, Z.; Wei, T.; Zhang, L. High-Performance Supercapacitor Electrodes Based on Highly Corrugated Graphene Sheets. *Carbon* **2012**, *50*, 2179−2188.

(21) Fan, Z.; Liu, Y.; Yan, J.; Ning, G.; Wang, Q.; Wei, T.; Zhi, L.; Wei, F. Template-Directed Synthesis of Pillared-Porous Carbon Nanosheet Architectures: High-Performance Electrode Materials for Supercapacitors. *Adv. Energy Mater.* **2012**, *2*, 419−424.

(22) Wang, H.; Xu, Z.; Kohandehghan, A.; Li, Z.; Cui, K.; Tan, X.; Stephenson, T. J.; King'ondu, C. K.; Holt, C. M. B.; Olsen, B. C.; Tak, J. K.; Harfield, D.; Anyia, A. O.; Mitlin, D. Interconnected Carbon Nanosheets Derived from Hemp for Ultrafast Supercapacitors with High Energy. *ACS Nano* **2013**, *7*, 5131−5141.

(23) Sevilla, M.; Fuertes, A. B. Direct Synthesis of Highly Porous Interconnected Carbon Nanosheets and Their Application as High-Performance Supercapacitors. *ACS Nano* **2014**, *8*, 5069−5078.

(24) Sevilla, M.; Fuertes, A. B. A General and Facile Synthesis Strategy Towards Highly Porous Carbons: Carbonization of Organic Salts. *J. Mater. Chem. A* **2013**, *1*, 13738−13741.

(25) Kruk, M.; Jaroniec, M.; Sayari, A. Application of Large Pore MCM-41 Molecular Sieves to Improve Pore Size Analysis Using Nitrogen Adsorption Measurements. *Langmuir* **1997**, *13*, 6267−6273.

(26) Neimark, A. V.; Lin, Y.; Ravikovitch, P. I.; Thommes, M. Quenched Solid Density Functional Theory and Pore Size Analysis of Micro-mesoporous Carbons. *Carbon* **2009**, *47*, 1617−1628.

(27) Ravikovitch, P. I.; Neimark, A. V. Density Functional Theory Model of Adsorption on Amorphous and Microporous Silica Materials. *Langmuir* **2006**, *22*, 11171−11179.

(28) Lillo-Ródenas, M. A.; Cazorla-Amorós, D.; Linares-Solano, A. Understanding Chemical Reactions between Carbons and NaOH and KOH: An Insight into the Chemical Activation Mechanism. *Carbon* **2003**, *41*, 267−275.

(29) Lillo-Ródenas, M. A.; Juan-Juan, J.; Cazorla-Amorós, D.; Linares-Solano, A. About Reactions Occurring During Chemical Activation with Hydroxides. *Carbon* **2004**, *42*, 1371−1375.

(30) Wang, J.; Kaskel, S. Koh Activation of Carbon-Based Materials for Energy Storage. *J. Mater. Chem.* **2012**, *22*, 23710−23725.

(31) Raymundo-Piñero, E.; Azaïs, P.; Cacciaguerra, T.; Cazorla-Amorós, D.; Linares-Solano, A.; Béguin, F. KOH and NaOH Activation Mechanisms of Multiwalled Carbon Nanotubes with Different Structural Organisation. *Carbon* **2005**, *43*, 786−795.

(32) McEnaney, B. In *Handbook of Porous Solids*; Wiley−VCH Verlag GmbH: Weinheim, Germany, 2008; pp 1828−1863.

(33) Matos, J. R.; Mercuri, L. P.; Kruk, M.; Jaroniec, M. Synthesis of Large-Pore Silica with Cage-like Structure Using Sodium Silicate and Triblock Copolymer Template. *Langmuir* **2002**, *18*, 884−890.

(34) Kruk, M.; Antochshuk, V.; Matos, J. R.; Mercuri, L. P.; Jaroniec, M. Determination and Tailoring the Pore Entrance Size in Ordered Silicas with Cage-like Mesoporous Structures. *J. Am. Chem. Soc.* **2002**, *124*, 768−769.

(35) Wei, L.; Sevilla, M.; Fuertes, A. B.; Mokaya, R.; Yushin, G. Hydrothermal Carbonization of Abundant Renewable Natural Organic Chemicals for High-Performance Supercapacitor Electrodes. *Adv. Energy Mater.* **2011**, *1*, 356−361.

(36) Taberna, P. L.; Simon, P.; Fauvarque, J. F. Electrochemical Characteristics and Impedance Spectroscopy Studies of Carbon−Carbon Supercapacitors. *J. Electrochem. Soc.* **2003**, *150*, A292−A300.

(37) Portet, C.; Taberna, P. L.; Simon, P.; Flahaut, E.; Laberty-Robert, C. High Power Density Electrodes for Carbon Supercapacitor Applications. *Electrochim. Acta* **2005**, *50*, 4174−4181.

(38) Enterria, M.; Castro-Muniz, A.; Suarez-Garcia, F.; Martinez-Alonso, A.; Tascon, J. M. D.; Kyotani, T. Effects of the Mesostructural Order on the Electrochemical Performance of Hierarchical Micro-Mesoporous Carbons. *J. Mater. Chem. A* **2014**, *2*, 12023−12030.

(39) Han, Y.; Liu, S.; Li, D.; Li, X. Three-Dimensionally Hierarchical Porous Carbon Creating High-Performance Electrochemical Capacitors. *Electrochim. Acta* **2014**, *138*, 193−199.

(40) Kötz, R.; Carlen, M. Principles and Applications of Electrochemical Capacitors. *Electrochim. Acta* **2000**, *45*, 2483−2498.

(41) Ma, X. M.; Gan, L. H.; Liu, M. X.; Tripathi, P. K.; Zhao, Y. H.; Xu, Z. J.; Zhu, D. Z.; Chen, L. W. Mesoporous Size Controllable Carbon Microspheres and Their Electrochemical Performances for Supercapacitor Electrodes. *J. Mater. Chem. A* **2014**, *2*, 8407−8415.

(42) Puthusseri, D.; Aravindan, V.; Madhavi, S.; Ogale, S. 3D Microporous Conducting Carbon Beehive by Single Step Polymer Carbonization for High Performance Supercapacitors: The Magic of In Situ Porogen Formation. *Energy Environ. Sci.* **2014**, *7*, 728−735.

(43) Sun, L.; Tian, C.; Fu, Y.; Yang, Y.; Yin, J.; Wang, L.; Fu, H. Nitrogen-Doped Porous Graphitic Carbon as an Excellent Electrode Material for Advanced Supercapacitors. *Chem.—Eur. J.* **2014**, *20*, 564−574.

(44) Qian, W.; Sun, F.; Xu, Y.; Qiu, L.; Liu, C.; Wang, S.; Yan, F. Human Hair-Derived Carbon Flakes for Electrochemical Supercapacitors. *Energy Environ. Sci.* **2014**, *7*, 379−386.

(45) Maxwell Technologies. *Application Note, Life Duration Estimation*; http://www.maxwell.com.

(46) Kötz, R.; Sauter, J. C.; Ruch, P.; Dietrich, P.; Büchi, F. N.; Magne, P. A.; Varenne, P. Voltage Balancing: Long-Term Experience with the 250 V Supercapacitor Module of the Hybrid Fuel Cell Vehicle Hy-Light. *J. Power Sources* **2007**, *174*, 264−271.

(47) Fuertes, A. B.; Lota, G.; Centeno, T. A.; Frackowiak, E. Templated Mesoporous Carbons for Supercapacitor Application. *Electrochim. Acta* **2005**, *50*, 2799−2805.

(48) Kierzek, K.; Frackowiak, E.; Lota, G.; Gryglewicz, G.; Machnikowski, J. Electrochemical Capacitors Based on Highly Porous Carbons Prepared by KOH Activation. *Electrochim. Acta* **2004**, *49*, 515−523.

(49) Ricketts, B. W.; Ton-That, C. Self-Discharge of Carbon-Based Supercapacitors with Organic Electrolytes. *J. Power Sources* **2000**, *89*, 64−69.